

# Redox Behavior of $(\text{CuO})_{0.15}(\text{CeO}_2)_{0.85}$ Mixed Oxide Catalyst Prepared by Sol-Gel Peroxide Method

Albin Pintar, Jurka Batista, and Stanko Hočevar\*

Laboratory for Catalysis and Chemical Reaction Engineering, National Institute of Chemistry, Hajdrihova 19, P.O. Box 660, SI-1001 Ljubljana, Slovenia

Received 17-08-2004

## Abstract

Temperature-programmed reduction (TPR), oxidation (TPO) and desorption (TPD) studies were performed on  $(\text{CuO})_{0.15}(\text{CeO}_2)_{0.85}$  copper-ceria mixed oxide sample prepared by sol-gel peroxide route. The obtained results reveal that despite initial drop in specific surface area after consecutive redox cycles the hydrogen consumption remains constant. This is because CuO is highly dispersed over the surface of  $\text{CeO}_2$  nano-crystallites and remains highly dispersed even after the agglomeration of  $\text{CeO}_2$  nano-crystallites in more dense secondary structure. The dispersed CuO is reduced to  $\text{Cu}^0$  during the TPR, forming agglomerated metal particles on the surface of partially reduced  $\text{CeO}_2$ . After subsequent TPO step all the  $\text{Cu}^0$  is oxidized back into CuO and re-dispersed over the  $\text{CeO}_2$  crystallites.

**Key words:** catalyst,  $(\text{CuO})_{0.15}(\text{CeO}_2)_{0.85}$ , redox properties, TPR, TPO, TPD

## Introduction

Cerium oxide and  $\text{CeO}_2$ -containing materials have been extensively studied as a component of heterogeneous industrial catalysts or as a support for transition metals due to their superior chemical and physical stability, high oxygen mobility, strong interaction with the supported metal and ability to be modified. Cerium oxide has been increasingly used as a thermal stabilizer and oxygen storage medium in the three-way catalysts for automotive emission control.<sup>1</sup>

$\text{CeO}_2$  has face-centered cubic crystal structure, into which various cation dopants can be introduced in order to improve the physicochemical properties of ceria.<sup>2–4</sup> The modification of  $\text{CeO}_2$  with  $\text{Cu}^{2+}$  ions leads to creation of oxygen ion vacancy around the  $\text{Cu}^{2+}$  ion in the  $\text{CeO}_2$ -based mixed oxide catalysts, to local structural changes and to decrease of the redox potentials of Cu species in the  $\text{CeO}_2$  matrix.<sup>5</sup> The obtained CuO- $\text{CeO}_2$  catalyst materials exhibited high activities for the oxidation of carbon monoxide and methane,<sup>6–8</sup> the  $\text{SO}_2$  reduction by CO,<sup>9–11</sup> the NO reduction<sup>12,13</sup>, the water gas shift reaction<sup>14</sup>, and the wet oxidation of phenol.<sup>15,16</sup> The CuO- $\text{CeO}_2$  mixed oxides were also reported to be highly active and selective for oxidation of carbon monoxide in excess of hydrogen.<sup>17–22</sup> The steam reforming of methanol over the Cu- $\text{CeO}_2$  catalysts, which were prepared by reduction of CuO- $\text{CeO}_2$  mixed oxides, was reported very recently.<sup>23–25</sup>

The catalysts for fundamental studies have been synthesized by various conventional techniques such as co-precipitation,<sup>2,6,9</sup> the urea co-precipitation/gela-

tion method,<sup>26</sup> the homogeneous co-precipitation using hexamethylenetetramine,<sup>27</sup> and by novel chemical routes such as the inert gas condensation technique,<sup>28–30</sup> and the solution combustion method.<sup>5</sup> The preparation conditions and mixed oxide composition influence the prevailing form and distribution of copper species on ceria. The enhanced catalyst activity and stability result from interactions between the copper-cerium oxide phases.

It was revealed that activity and selectivity of two series of  $(\text{CuO})_x(\text{CeO}_2)_{1-x}$  catalysts prepared by co-precipitation method and by sol-gel peroxide route increase with the dispersion of copper oxide phase on the cerium oxide.<sup>15,16</sup> A comparative study of Pt/ $\gamma$ - $\text{Al}_2\text{O}_3$ , Au/ $\alpha$ - $\text{Fe}_2\text{O}_3$  and  $(\text{CuO})_{0.05}(\text{CeO}_2)_{0.95}$  catalysts for the selective oxidation of carbon monoxide in excess hydrogen showed that the  $(\text{CuO})_{0.05}(\text{CeO}_2)_{0.95}$  catalyst prepared by the sol-gel peroxide route is superior to the other two catalysts in the low-temperature range, because it has the best compromise between activity, selectivity, and price of the catalyst.<sup>18</sup> The kinetics of selective CO oxidation in excess of hydrogen over the  $(\text{CuO})_{0.1}(\text{CeO}_2)_{0.9}$  nanostructured catalyst prepared by sol-gel peroxide route was studied under simulated preferential oxidation (PROX) reactor conditions.<sup>19</sup>

In this work, we report on the examination of a  $(\text{CuO})_{0.15}(\text{CeO}_2)_{0.85}$  mixed oxide catalyst (synthesized by the modified sol-gel technique using hydrogen peroxide<sup>16</sup> and referred to as CuCe-2) by means of TPR, TPO and TPD techniques, which will be demonstrated as an efficient tool to obtain information about the redox behavior of this solid, understanding of which is of

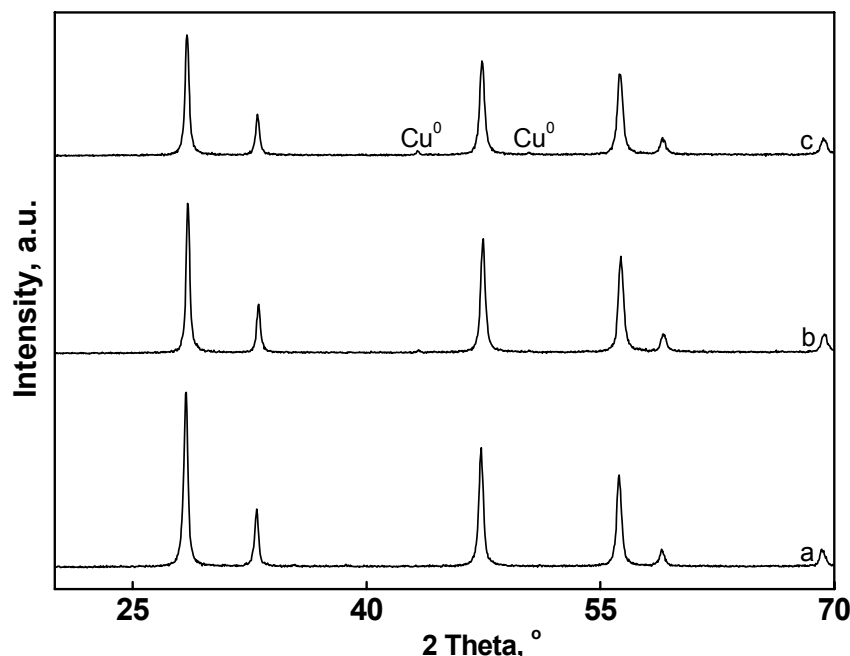


**Figure 1.** X-ray powder diffraction patterns of CuCe-2 sample: (a) fresh; (b) after TPR-1/TPO/TPR-2 analysis; (c) after four consecutive TPR/TPO cycles.

practical importance for designing CuO-CeO<sub>2</sub> catalysts that can replace the expensive noble metal catalysts in a number of down-stream processes for production of H<sub>2</sub>-rich gas streams from fossil and renewable fuels used as a fuel for the proton exchange membrane fuel cells (PEMFC).

## Results and discussion

### 1. X-ray diffraction analysis and UV-VIS spectroscopy

X-Ray powder diffraction patterns of fresh and treated CuCe-2 mixed oxide samples are shown in Figure 1. The X-ray pattern of fresh CuCe-2 sample revealed the characteristic diffraction peaks of CeO<sub>2</sub> phase (Cerianite, syn, cubic, PDF 34-0394:  $2\theta = 28.6, 33.1, 47.5, 56.3, 59.1$  and  $69.4^\circ$ ), assigned to the fluorite structure. The single-phase XRD patterns indicate a high dispersion of copper species (X-ray amorphous) at the surface of CeO<sub>2</sub> crystallites. The diffraction peaks of cerianite in CuCe-2 sample prepared by sol-gel peroxide route are strong and sharp, which means that the CuO phase is finely dispersed on the surface of relatively large CeO<sub>2</sub> crystallites.<sup>16</sup> By peak broadening analysis, the average crystallite size in the direction normal to the (111) plane in cerianite was calculated to be 42 nm.

In order to obtain preliminary information on the copper species present in the CuCe-2 sample, UV-VIS diffuse reflectance spectra of the reference CeO<sub>2</sub>, CuO and Cu<sub>2</sub>O materials and prepared mixed oxide were collected. The positions of the absorption maxima for CuO ( $\lambda = 875$  nm) and Cu<sub>2</sub>O ( $\lambda = 620$  nm) clearly demonstrate

the presence of the d-d transitions of Cu<sup>2+</sup> (3d<sup>9</sup>) in the examined mixed oxide sample.<sup>31</sup>

### 2. H<sub>2</sub>-TPR, O<sub>2</sub>-TPO, TPD-H<sub>2</sub> and TPD-O<sub>2</sub>

Interaction of hydrogen with (CuO)<sub>x</sub>(CeO<sub>2</sub>)<sub>1-x</sub> mixed oxides during TPR involves the adsorption of hydrogen on all active sites of the cerium oxide surface, storage of hydrogen in the host oxide and reduction of the CuO component.<sup>27,32–34</sup> The qualitative and quantitative characterization of reducibility and reoxidability of different types (*i.e.*, well-dispersed, bulk-like) of copper ions present in the prepared CuCe-2 mixed oxide are determined by TPR and TPO measurements carried out in the temperature range from 0 to 400 °C (Figure 2). Figure 2a confirms that highly dispersed copper ions in nanocrystalline (CuO)<sub>0.15</sub>(CeO<sub>2</sub>)<sub>0.85</sub> can be readily reduced and oxidized at temperatures as low as 260 °C.<sup>35</sup> The extent of further reoxidation of Cu<sup>0</sup> to Cu<sup>2+</sup>, partial consumption of hydrogen stored in reduced samples and storage of oxygen during the TPO run are illustrated in Figure 2b. The numerical values of the TPR and TPO peak areas of the copper-cerium oxide sample (Figure 2) are evaluated and listed in Table 1. Comparison of TPR profiles of CuCe-2 sample obtained by carrying the TPR experiments at different sample loading (0.10 and 0.25 g, respectively) confirms the reproducibility of TPR profile characteristics: the temperature corresponding to the maximum reduction rate and the shape of the TPR profile. At the same time peak area increases proportionally with increasing sample loading, which implies that the reduction profile is not influenced by

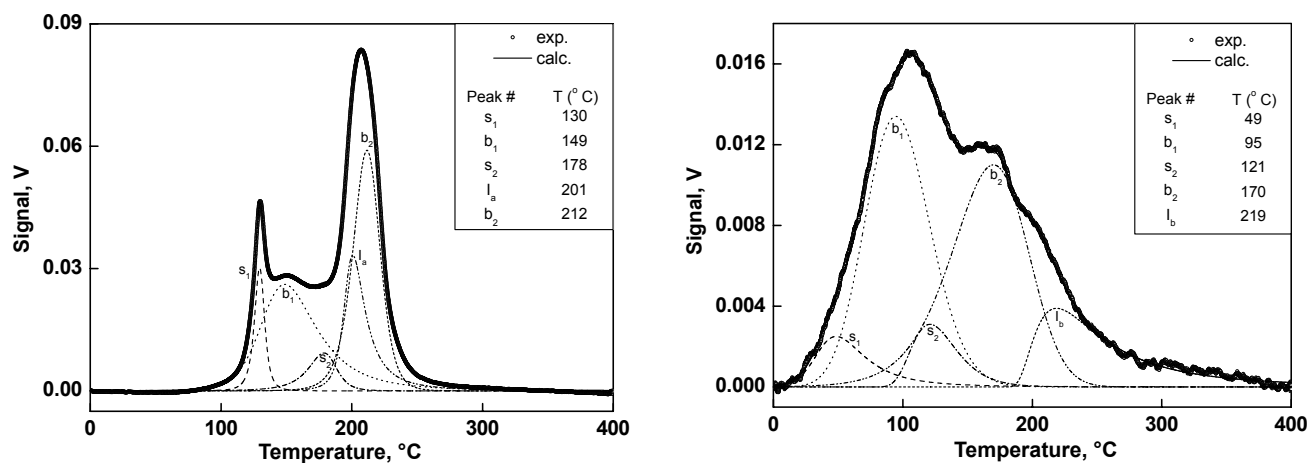


**Figure 2.** TPR-1 (a) and TPO (b) profiles of CuCe-2 sample measured in the temperature range of 0–400 °C and predicted by means of deconvolution method. Operating conditions: 50 mL/min (STP), H<sub>2</sub>(5 vol.%)/Ar (a), O<sub>2</sub>(10 vol.%)/He (b), 5 °C/min. Sample weight: 250 mg. The initial state of (b) is fresh sample following TPR-1 run, cooling in H<sub>2</sub>(5 vol.%)/Ar to 0 °C and purging at 0 °C with pure Ar. Designation of peaks: s<sub>1</sub> – partial reduction of Cu<sup>2+</sup> → Cu<sup>+</sup> in well-dispersed CuO species; s<sub>2</sub> – partial reduction of Cu<sup>+</sup> → Cu<sup>0</sup> in well-dispersed CuO species; b<sub>1</sub> – partial reduction of Cu<sup>2+</sup> → Cu<sup>+</sup> in bulk-like CuO phase; b<sub>2</sub> – partial reduction of Cu<sup>+</sup> → Cu<sup>0</sup> in bulk-like CuO phase. I<sub>a</sub> – H<sub>2</sub> incorporation in the catalyst structure; I<sub>b</sub> – consumption of H<sub>2</sub> incorporated in the catalyst structure during the TPR-1 analysis.

the operating conditions (*i.e.*, initial amount of reducible species, heating rate).<sup>36</sup>

In order to verify the restoration of redox properties of examined mixed oxide, the second TPR run was performed following TPO after cooling the sample in helium flow to 0 °C. TPR-2 measurement was carried out under the same reaction conditions as the first TPR-1 run. The TPR-1/TPO/TPR-2 cycling of CuCe-2 revealed that the TPR profile characteristics are not reproducible (Figure 3a). We observed in accordance with the findings of Zimmer *et al.*<sup>27</sup> that heat treatment under hydrogen (TPR-1 analysis) reduces the specific surface area of CuCe-2 from 31 to 26 m<sup>2</sup>/g; no further decrease of specific surface area was observed in subsequent TPR/TPO cycles. However, a comparison of the XRD patterns for prepared and TPR-1/TPO/TPR-2 treated CuCe-2 samples (Figure 1) provide no evidence that such treatment has substantial influence on the changing of the cerium oxide diffraction peaks. A weak XRD peak associated with the Cu<sup>0</sup> phase is slightly above the detection limit. Apparently, XRD was not sensitive to the dispersed copper component.

### 2.1. Quantitative analysis

For quantitative analysis, all of the TPR, TPO and TPD peaks that can be discerned by computer software (Grams/32, Thermo Galactic, version 4) have been integrated to evaluate their individual amounts. The numerical values obtained from the integrated areas are given in Table 1. Baseline correction and deconvolution of TPR and TPO profiles with five peaks using the PeakFit software package (SPSS, version 4.11) give the area percentage for the copper ion species closely

interacting with the cerium oxide and for the segregated (bulk-like) CuO.

Evidently, the total hydrogen consumption of CuCe-2 solid is larger than the value expected for a complete reduction of the CuO component to Cu<sup>0</sup> (Table 1). The additional hydrogen consumption may be due to surface reduction of CeO<sub>2</sub>.<sup>27,32–34</sup> During the reduction process, storage of hydrogen in the oxide, mainly in the bulk (*i.e.*, formation of bronze-like species) and further reaction of these activated hydrogen species with the lattice oxygen ions at T > 230 °C can take place.<sup>34</sup> Furthermore, it was reported that the incorporation of Ni<sup>2+</sup> or Cu<sup>2+</sup> in ceria affects the hydrogen storage in the host oxide and the degree of reduction of the cations.<sup>33,37</sup> In order to determine the amount of hydrogen stored in the host oxide (HSC), the calculated amount of H<sub>2</sub>, which is needed for complete reduction of CuO to Cu<sup>0</sup> and the amount of hydrogen that reacts with oxygen stored in copper-cerium mixed oxide (after activation) is subtracted from the total hydrogen uptake (TPR). The obtained H<sub>2</sub> consumption is then compared with the amount of hydrogen desorbed from reduced solid in the same temperature range (TPD-H<sub>2</sub>). Quantitative analysis of the TPO profiles revealed the extent of reoxidation of Cu<sup>0</sup> on reduced CuCe-2 sample, the part of stored hydrogen that reacts with oxygen during temperature-programmed oxidation and the amount of oxygen stored in the sample during TPO.

Figure 2a shows that the CuCe-2 sample starts to be reduced at temperatures below 100 °C. The reduction steps as well as the simultaneous incorporation of hydrogen into the catalyst structure is completed at temperatures below 260 °C. Data shown in Table 1

**Table 1.** Results of TPR-1, TPO, TPR-2, TPD-H<sub>2</sub> and TPD-O<sub>2</sub> analyses of CuCe-2 sample.

Analyses	CuCe-2	Analyses	CuCe-2
TPR-1		<i>TPD-H<sub>2</sub> up to 650 °C</i>	
total H <sub>2</sub> uptake, mL/g <sub>solid</sub>	25.2	desorbed H <sub>2</sub> , mL/g <sub>solid</sub>	4.0 <sup>d</sup>
stored H <sub>2</sub> (HSC <sub>1</sub> ), mL/g <sub>solid</sub>	4.0 (16%) <sup>d</sup>	rest of H <sub>2</sub> , mL/g <sub>solid</sub>	0
TPO		irreversibly captured H <sub>2</sub> , %	
total O <sub>2</sub> uptake, mL/g <sub>solid</sub>	12.6	<i>TPD-H<sub>2</sub> up to 400 °C</i>	
partial O <sub>2</sub> uptake, mL/g <sub>solid</sub>	2.0 (16%) <sup>b</sup>	desorbed H <sub>2</sub> , mL/g <sub>solid</sub>	3.2
remained H <sub>2</sub> , mL/g <sub>solid</sub>	0.0 (0%) <sup>c</sup>	rest of H <sub>2</sub> , mL/g <sub>solid</sub>	0.8
TPR-2		irreversibly captured H <sub>2</sub> , %	
total H <sub>2</sub> uptake, mL/g <sub>solid</sub>	25.2	<i>TPD-O<sub>2</sub> up to 400 °C</i>	
stored H <sub>2</sub> (HSC <sub>2</sub> ), mL/g <sub>solid</sub>	4.0	desorbed O <sub>2</sub> , mL H <sub>2</sub> /g <sub>solid</sub>	1.3
HSCC, mL/g <sub>solid</sub>	≈ 4.0		

<sup>a</sup> Part of H<sub>2</sub> consumed for incorporation into the catalyst structure. <sup>b</sup> Part of O<sub>2</sub> consumed in a reaction with H<sub>2</sub> stored in the catalyst structure. <sup>c</sup> Part of H<sub>2</sub> stored in the catalyst structure after the completion of TPO analysis. <sup>d</sup> The same value was measured during the TPD analysis conducted after four TPR/TPO cycles.

confirm that in the performed TPR analysis complete reduction of CuO phases was obtained. At a first sight, at least three peaks could be distinguished on the TPR profile of CuCe-2: the first peak with a maximum at T = 135 °C, the second one at T = 158 °C and a large reduction peak with a maximum at 212 °C (Figure 2a). The total hydrogen uptake obtained from the integrated area is 25.2 mL H<sub>2</sub>/g<sub>solid</sub>, which is equivalent to the stoichiometric total oxygen consumption of 12.6 mL O<sub>2</sub>/g<sub>solid</sub> (Table 1). Assuming all the Cu content (x = 0.15) in the activated CuCe-2 solid is present as CuO, 21.2 mL H<sub>2</sub>/g<sub>solid</sub> is required to reduce CuO to Cu<sup>0</sup>. The excess hydrogen uptake of 4.0 mL H<sub>2</sub>/g<sub>solid</sub> is calculated as the difference between the total amount of consumed H<sub>2</sub> and the amount of H<sub>2</sub> needed for complete reduction of Cu<sup>2+</sup> ions in the CuCe-2. After hydrogen uptake up to 400 °C, the CuCe-2 was cooled in H<sub>2</sub> and purged with Ar, and then the temperature-programmed desorption of hydrogen was carried out. The obtained amount of H<sub>2</sub> desorbed from CuCe-2 in the temperature range up to 400 °C is 3.2 mL H<sub>2</sub>/g<sub>solid</sub> (Table 1). This means that about 20% of stored hydrogen remains irreversibly captured in the CuCe-2 solid after treatment up to 400 °C. Temperature-programmed oxidation of reduced CuCe-2 gives the TPO signal consisting of five overlapping peaks with maxima at 49, 95, 121, 170, and 219 °C (Figure 2b). The excess oxygen uptake of 2.0 mL O<sub>2</sub>/g<sub>solid</sub> (Table 1) can be ascribed to the extraction of stored hydrogen from the CuCe-2 previously reduced up to 400 °C (Figure 2a). Comparison of the total hydrogen uptake with the total oxygen consumption shows that 0.0 mL H<sub>2</sub>/g<sub>solid</sub> was remained in the CuCe-2 solid after TPR/TPO runs (Table 1).

Subsequently, deconvolution of TPR profile illustrated in Figure 2a was performed. Among numer-

ous functions tested, the best agreement between the measured and calculated TPR profiles was obtained by using the Pearson IV fit function allowing asymmetric peaks. It can be seen that excellent agreement between the measured and predicted TPR profiles was obtained in the whole temperature range. Five peaks were sufficient to accurately describe H<sub>2</sub> consumption during the reduction of CuCe-2 sample. This suggests that in the stepwise hydrogenation of CuO the reduction of intermediate Cu<sup>+</sup> phases to Cu<sup>0</sup> proceeds at a comparable rate in comparison to the Cu<sup>2+</sup> → Cu<sup>+</sup> reduction step. The mathematical analysis of TPR profile illustrated in Figure 2a reveals that the storage of H<sub>2</sub> into the catalyst structure occurs in parallel to the reduction of CuO or Cu<sub>2</sub>O phases. The peak that shows the course of H<sub>2</sub> storage as a function of temperature is marked in Figure 2a with letter I (incorporated). Although hydrogen can be stored in the examined catalyst in various forms,<sup>32–34</sup> no attempt was made during the mathematical analysis of TPR profiles illustrated in Figure 2a to further deconvolute I curve and thus try to differentiate between various processes contributing to hydrogen storage capacity. This is because the measured TPR profiles were rather smooth not exhibiting many obvious peaks, which would be needed to perform deconvolution of I curve. It is interesting to note that the amount of H<sub>2</sub> incorporated into the catalyst structure, calculated by means of the performed deconvolution analysis, is in good agreement with the results of TPR analysis (Table 1). For example, the performed simulation shows that 18% of H<sub>2</sub> consumed (I<sub>a</sub> peak in Figure 2a) was incorporated into the catalyst structure; based on the results of TPR-1 analysis, this value equals to 16% (Table 1). The performed deconvolution analysis can be also used to estimate the amount of well-dispersed CuO species

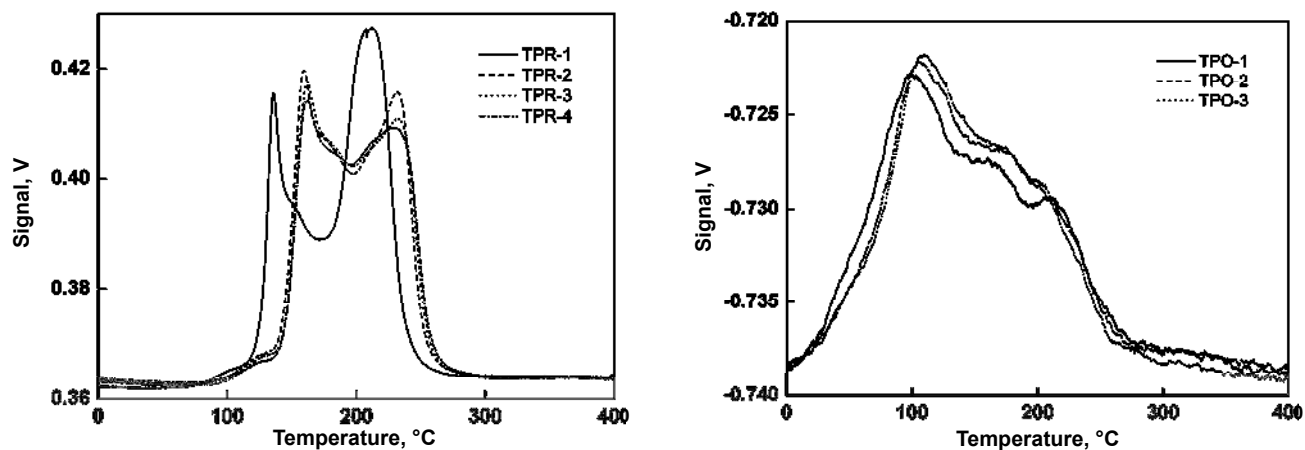


**Figure 3.** Comparisons of TPR and TPO patterns obtained in the temperature range of 0–400 °C of CuCe-2 mixed oxide treated in consecutive TPR/TPO cycles. For operating conditions, see Figure 1. Sample weight: 250 mg.

(sum of  $s_1$  and  $s_2$  relative peak areas, 15%) and bulk-like CuO species on the surface of CeO<sub>2</sub> crystallites (sum of  $b_1$  and  $b_2$  relative peak areas, 85%), which was confirmed recently by N<sub>2</sub>O selective chemisorption analysis.<sup>38</sup>

Figure 2b shows a profile obtained during the TPO analysis of pre-reduced CuCe-2 sample. It should be noted that no oxygen was consumed at  $T \leq 0$  °C. It was also verified by means of pulse chemisorption measurements carried out at  $T = 0$  °C that no O<sub>2</sub> was consumed during the preceding detector stabilization period (5 min), in which a catalyst sample was exposed to oxygen stream. It can be further seen that in comparison to TPR analysis the catalyst reoxidation completes at temperatures similar to the ones required for complete reduction of this solid. As discussed below, the oxidative treatment at temperatures up to 400 °C is sufficient for the examined catalyst sample to completely reoxidize the copper phases. The TPO profile measured during the reoxidation of CuCe-2 sample (Figure 2b) was satisfactorily simulated by assuming the following processes: (i) reoxidation of the well dispersed Cu phase; (ii) reoxidation of the segregated Cu phase; (iii) consumption of H<sub>2</sub> stored in the catalyst structure. An involvement of five peaks was required to satisfactorily simulate the measured TPO profile during the subsequent deconvolution. This is in agreement with results of TPR analysis illustrated in Figure 2a, during which stepwise reduction of CuO was observed. Peaks  $s_1$  and  $s_2$  in Figure 2b are attributed to the stepwise reoxidation of well-dispersed Cu phase, while peaks  $b_1$  and  $b_2$  belong to the reoxidation of bulk-like Cu phase. The calculated areas of peaks of each pair are very similar. The calculated relative surface areas of peaks belonging to the reoxidation of well dispersed (14%) and segregated (86%) Cu phases, are very close to the corresponding TPR-1 values. Furthermore, the calculated relative area of peak  $I_b$ , demonstrating the consumption of incorporated H<sub>2</sub>

during the TPO analysis, was found to be equal to 14%, which is again very close to the measured value of 16% calculated on the basis of data listed in Table 1. Finally, it is reported in Table 1 that in CuCe-2 sample, which exhibits rather low HSC capacity, hydrogen stored in the catalyst during the preceding TPR step was completely consumed during the TPO analysis.

The second reduction of catalyst sample examined in this study was performed and compared to those measured during the TPR-1 analysis (see Figure 3a). It was found out that the TPR-2 profile is shifted towards higher temperatures. This shift is the consequence of substantial decrease of the sample volume (up to 15%), which occurred during the TPR-1 analysis. This causes different bulk density as well as different location of the thermocouple in the sample bed. Consequently, the lower heat transfer to thermocouple by the gas convection in comparison with the heat transfer by conduction causes shift to higher temperature. Partially, the shift might be attributed also to the fact that the BET surface area drops after TPR-1 analysis (from 31 to 26 m<sup>2</sup>/g). Interestingly, the same number of peaks (5) was used to satisfactorily simulate the TPR-2 profile by means of the deconvolution method as was in the case of TPR-1 analysis. This analysis, which accurately takes into account the amount of hydrogen incorporated in the catalyst structure during the TPR-2 analysis (Table 1), interestingly shows that the percentage of well-dispersed and bulk-like CuO phases remains constant in the applied temperature range. Although the BET surface area changes during the TPR-1 analysis, these findings suggest that the interface between the CuO and CeO<sub>2</sub> phases is not modified significantly. Furthermore, additional TPR/TPO cycles illustrated in Figure 3 reveal that total hydrogen and oxygen consumptions as well as HSC values remain constant in consecutive TPR/TPO cycles. It is believed that this is due to high dispersion of

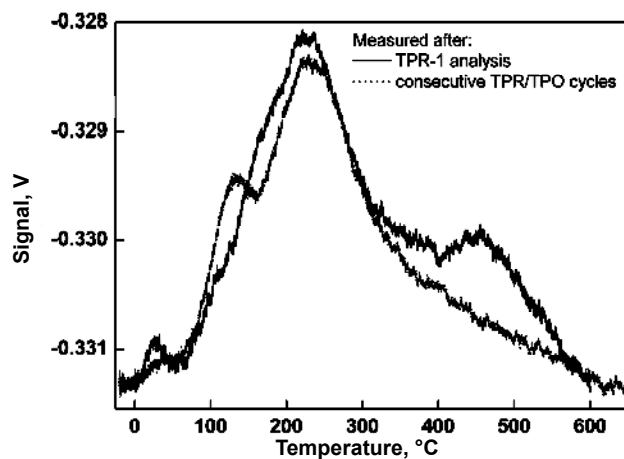


**Figure 4.** Comparison of TPD- $H_2$  patterns of CuCe-2 sample obtained in the temperature range of  $-20$ – $650$  °C after TPR-1 analysis or consecutive TPR/TPO cycles carried out up to  $400$  °C. Operating conditions:  $50$  mL/min (STP), pure Ar,  $5$  °C/min. Sample weight:  $250$  mg.

CuO over the surface of  $CeO_2$  nano-crystallites, which is maintained even after the agglomeration of  $CeO_2$  nano-crystallites in more dense secondary structure. This is confirmed by the fact that subsequent TPR-2 – TPR-4 profiles (Figure 3a) as well as TPO-2 – TPO-3 patterns (Figure 3b) are not shifted to higher temperatures.

It is evident from Table 1 that rather low quantity of hydrogen was stored in the structure of CuCe-2 sample during the TPR-1 analysis. It is also shown that hydrogen initially incorporated in CuCe-2 sample was completely consumed in the subsequent reoxidation step conducted in the temperature range of  $0$ – $400$  °C. Since the amounts of hydrogen consumed during the TPR-1 and TPR-2 analyses of CuCe-2 sample were found to be equal, this means that the complete hydrogen storage capacity (HSCC) of this solid was achieved in the first reduction step. On the basis of performed analysis, it is concluded that the HSCC for CuCe-2 sample is equal to  $4.0$  mL  $H_2/g_{\text{solid}}$ .

TPD- $H_2$  profile of pre-reduced CuCe-2 sample (after TPR-1 analysis) was measured at temperatures up to  $650$  °C, which was sufficiently high so that the signal of TCD detector returned to the initial value. This analysis illustrated in Figure 4 reveals that very small amount of  $H_2$  was physisorbed on the catalyst surface (peak at approx.  $30$  °C) and that the majority of  $H_2$  stored in the catalyst during the TPR analysis was chemisorbed.  $H_2$  desorption occurred in a wide temperature range, and two wide peaks are noted. However, in the applied temperature interval, complete desorption of  $H_2$  incorporated in the catalyst structure was achieved. This was confirmed also by TPD- $H_2$  examination of CuCe-2 sample, previously used in four TPR/TPO cy-

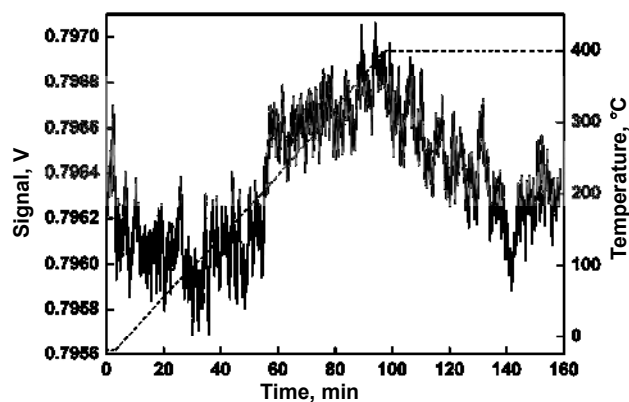


**Figure 5.** TPD- $O_2$  pattern of CuCe-2 sample measured in the temperature range of  $-20$ – $400$  °C. Operating conditions:  $50$  mL/min (STP), pure He,  $5$  °C/min. Sample weight:  $250$  mg.

cles; a profile similar to the one measured after TPR-1 analysis was obtained (Figure 4). By means of TPD analysis of CuCe-2 sample subjected to consecutive TPR/TPO cycling, the same HSCC value as reported above was obtained. It was estimated on the basis of presented TPD spectra (and confirmed by additional TPD experiments) that about  $80\%$  of  $H_2$  was desorbed from CuCe-2 sample at temperatures up to  $400$  °C. Since hydrogen incorporated in the catalyst structure was completely consumed during the TPO analysis, carried out by means of diluted oxygen stream in the temperature range of  $0$ – $400$  °C, this implies that higher temperatures are obviously required to achieve complete hydrogen desorption when the catalyst sample is purged by inert gas. Finally, it is very interesting to note that the locations of peak maxima in measured TPD- $H_2$  profiles (Figure 4), which appear in the temperature range of  $150$ – $250$  °C, are in very good agreement with the location of peak in predicted  $I_b$  curve, showing the consumption of oxygen in TPO experiment that reacted with stored hydrogen (Figure 2b).

The TPD- $O_2$  profile illustrated in Figure 5 for CuCe-2 sample pre-calcined at  $400$  °C lies in a very short range of TCD signals, which alludes that in the applied temperature range of  $-20$ – $400$  °C the examined solid exhibits, in comparison to measured TPD- $H_2$  values, lower ability for the exchange of oxygen. The amount of desorbed oxygen for given temperature range is listed in Table 1. It is seen that TPD- $O_2$  value is about  $3$  times lower compared with TPD- $H_2$  data obtained in the same temperature range. However, the reported TPD- $O_2$  value is in good agreement with data found in the literature.<sup>39</sup> Finally, hydrogen pulse chemisorption

measurements of CuCe-2 sample after TPD-O<sub>2</sub> treatment (not shown) confirmed that no chemisorption of hydrogen occurred at temperature close to 0 °C.

## Conclusions

The results of this study reveal that despite a drop in specific surface area of CuCe-2 mixed oxide sample after the first TPR-H<sub>2</sub> treatment, which implies that morphological changes take place, the redox behavior of this solid prepared by the sol-gel peroxide route remains nearly unchanged as total hydrogen consumption, hydrogen storage capacity and total oxygen consumption remain constant during successive TPR/TPO cycles.

During the TPR-1 analysis the CuO, which is X-ray amorphous and dispersed over the CeO<sub>2</sub> crystallites (with dimension of about 42 nm), reduces to Cu<sup>0</sup>. The Cu<sup>0</sup> phase can be detected by X-ray diffraction after the reduction process. This means that the reduction process is accompanied by metal particles agglomeration process. However, after subsequent TPO the Cu<sup>0</sup> is again oxidized back into CuO and re-dispersed over the CeO<sub>2</sub> crystallites. Consequently, in subsequent reduction/oxidation cycles the TPR and TPO patterns are not shifted towards higher temperatures.

## Experimental

### 1. Preparation of (CuO)<sub>0.15</sub>(CeO<sub>2</sub>)<sub>0.85</sub> mixed oxide sample (CuCe-2)

CuCe-2 sample was prepared by sol-gel peroxide route method<sup>15</sup> by reacting CuCl<sub>2</sub>·2H<sub>2</sub>O (99 wt.% purity, Aldrich) with H<sub>2</sub>O<sub>2</sub> water solution (30 wt.%, p.a., Merck) and in separate vessel by reacting H<sub>2</sub>O<sub>2</sub> water solution with CeCl<sub>3</sub>·7H<sub>2</sub>O (99.9 wt.% purity, Aldrich). The concentration of metal chloride in aqueous H<sub>2</sub>O<sub>2</sub> solution was altered to attain the desired (Cu:Ce) molar ratio in the oxide sample. After the reaction was completed, the solution was vigorously mixed and the excess peroxide was decomposed at about 60 °C and then the ethanol (molar ratio of ethanol to metallic ions = 30) was added slowly during continuous stirring at room temperature. The solvent was removed by evaporation at about 40 °C, and then the remaining viscous product was slowly dried to obtain the xerogel, which was calcined at 400 °C for 6 h in dry air.

### 2. Characterization

#### 2.1. X-ray diffraction analysis

The crystalline phases present in the prepared and treated CuCe-2 samples and the average crystallite sizes were examined by X-ray diffraction using a Philips PW-1710 diffractometer with Cu K $\alpha$  irradiation source ( $\lambda$  =

0.15406 nm) operated at 40 kV and 30 mA. The XRD patterns of samples were measured in 0.04° steps from 7 to 70° (in 2 $\theta$ ) with 1 s per step. The obtained patterns were compared with PDF data files<sup>40</sup> to confirm phase identities. The average crystallite sizes were calculated applying the Scherrer equation<sup>41</sup> to the line broadening of diffraction peak from (111) plane in cerianite.

#### 2.2. UV-VIS diffuse reflectance spectroscopy

Diffuse reflectance UV-VIS spectra of CuCe-2 sample as well as of reference materials were recorded at room temperature using a Perkin-Elmer Lambda 40P UV-VIS spectrophotometer equipped with the RSA-PE-19M Praying Mantis accessory, which is designed for diffuse reflectance measurements of horizontally positioned powder samples, pastes or rough surface samples. The Spectralon<sup>®</sup> white reflectance standard was used to perform the instrument background correction in the range of 200-900 nm. The scans were acquired in duplicates with speed of 120 nm/min and slit set to 4 nm.

#### 2.3. BET, TPR, TPO and TPD measurements

Single-point BET surface area, temperature-programmed reduction (TPR) with hydrogen, temperature-programmed oxidation (TPO) with oxygen, temperature-programmed desorption (TPD) of hydrogen, temperature-programmed desorption of oxygen, and hydrogen pulse chemisorption measurements of CuCe-2 sample were performed by means of an automated catalyst characterization system (Micromeritics, model AutoChem II 2920), which incorporates a thermal conductivity detector (TCD). The sample loadings were 0.10 and 0.25 g. Prior to BET analysis, the sample was degassed at 200 °C in He. Before starting TPR and TPD-O<sub>2</sub> runs, the sample was activated under flowing O<sub>2</sub>(10 vol.%)/He at 400 °C for 90 min. TPR, TPO and TPD experiments were carried out at a heating rate of 5 °C/min. The reactive gas compositions were H<sub>2</sub>(5 vol.%)/Ar for TPR and O<sub>2</sub>(10 vol.%)/He for TPO. The flow rate was fixed at 50 mL/min (STP). The total reactive gas consumption (TPR and TPO) and desorption (TPD-O<sub>2</sub> and TPD-H<sub>2</sub>) were measured. To convert the peak area data to volume data, the analyzer was calibrated with gas mixtures of known composition.

The TPR measurements were carried out following activation after cooling the sample in helium flow to 0 °C. The sample was then held at 0 °C under flowing helium to remove the remaining adsorbed oxygen so that the TCD signal returned to the baseline. Then the TPR experiments were performed up to a temperature 400 °C at which the sample was maintained for 30 min. The trap was cooled with isopropyl alcohol/liquid nitrogen slurry (IPA/LN<sub>2</sub>, T = -80 °C). In order to verify

that mass transfer limitations do not affect the TPR measurements, we have carried out TPR experiments at different sample loadings (*i.e.*, 0.10 and 0.25 g).

The TPO experiments were performed following TPR after cooling the samples in H<sub>2</sub>(5 vol.%) / Ar flow to 0 °C. The samples were then purged at 0 °C in flowing Ar to remove the residual hydrogen. After that O<sub>2</sub>(10 vol.%) / He gas mixture was passed over the samples which were heated to 400 °C and then held at 400 °C for 1 h.

To examine the reproducibility of TPR/TPO profiles after the reoxidation, the sample was cooled in helium flow to 0 °C at the end of the TPR-1/TPO cycle and then consecutive reduction/oxidation runs were carried out under the same reaction conditions as described above.

The TPD-H<sub>2</sub> was performed following the TPR experiments after cooling the reduced sample in H<sub>2</sub>(5 vol.%) / Ar gas mixture flow to –20 °C. At that temperature, the sample was maintained under flow of pure argon to remove the residual hydrogen so that the TCD signal returned to the baseline. After that the TPD-H<sub>2</sub> experiment was carried out up to a temperature of 650 °C, at which the sample was held for 30 min.

The TPD-O<sub>2</sub> was carried out on the activated sample, which was cooled in O<sub>2</sub>(10 vol.%) / He gas mixture flow to –20 °C and then purged in flowing helium to remove the residual oxygen. The TPD-O<sub>2</sub> measurement was performed up to a temperature of 400 °C, at which the sample was held for 6 h.

The hydrogen pulse chemisorption measurements of CuCe-2 sample were applied after TPD-O<sub>2</sub> measurements to find out whether a chemisorption of hydrogen occurred at temperature close to 0 °C (*i.e.*, during TPR runs). The sample was degassed and cooled under flowing argon to –5 °C, at which pulses of H<sub>2</sub>(5 vol.%) / Ar were injected into a stream of Ar flowing through the sample bed. The injection loop (nominal volume 0.5 mL) was calibrated with pulses of N<sub>2</sub> in helium flow and compared against a calibration line produced from gas tight syringe injections of N<sub>2</sub> under helium flow.

## Acknowledgements

The authors gratefully acknowledge the financial support of the Ministry of Education, Science and Sport of the Republic of Slovenia through Grant P1-0152-0104.

## References

1. A. Trovarelli, *Catal. Rev. - Sci. Eng.* **1996**, *38*, 439–520.
2. Y. Zhang, S. Andersson, M. Muhammed, *Appl. Catal. B* **1995**, *6*, 325–337.
3. P. Fornasiero, G. Balducci, R. Di Monte, J. Kaspar, V. Sergo, G. Gubitosa, A. Ferrero, M. Graziani, *J. Catal.* **1996**, *164*, 173–183.
4. A. E. C. Palmqvist, E. M. Johansson, S. G. Järas, M. Muhammed, *Catal. Lett.* **1998**, *56*, 69–75.
5. P. Bera, K. R. Priolkar, P. R. Sarode, M. S. Hegde, S. Emura, R. Kumashiro, N. P. Lalla, *Chem. Mater.* **2002**, *14*, 3591–3601.
6. W. Liu, M. Flytzani-Stephanopoulos, *J. Catal.* **1995**, *153*, 304–316.
7. Lj. Kundakovic, M. Flytzani-Stephanopoulos, *J. Catal.* **1998**, *179*, 203–221.
8. A. Martinez Arias, R. Cataluna, J. C. Conesa, J. Soria, *J. Phys. Chem. B* **1998**, *102*, 809–817.
9. W. Liu, A. F. Sarofim, M. Flytzani-Stephanopoulos, *Appl. Catal. B* **1994**, *4*, 167–186.
10. A. Tschöpe, W. Liu, M. Flytzani-Stephanopoulos, J. Y. Ying, *J. Catal.* **1995**, *157*, 42–50.
11. T. Zhu, Lj. Kundakovic, A. Dreher, M. Flytzani-Stephanopoulos, *Catal. Today* **1999**, *50*, 381–397.
12. M. Fernandez-Garcia, E. Gomez Rebollo, A. Guerrero Ruiz, J. C. Conesa, J. Soria, *J. Catal.* **1997**, *172*, 146–159.
13. P. Bera, S. T. Aruna, K. C. Patil, M. S. Hegde, *J. Catal.* **1999**, *186*, 36–44.
14. X. Qi, M. Flytzani-Stephanopoulos, *Ind. Eng. Chem. Res.* **2004**, *43*, 3055–3062.
15. S. Hočevar, J. Batista, J. Levec, *J. Catal.* **1999**, *184*, 39–48.
16. S. Hočevar, U. Opara Krašovec, B. Orel, A. S. Aricó, H. Kim, *Appl. Catal. B* **2000**, *28*, 113–125.
17. G. Avgouropoulos, T. Ioannides, H. K. Matralis, J. Batista, S. Hočevar, *Catal. Lett.* **2001**, *73*, 33–40.
18. G. Avgouropoulos, T. Ioannides, Ch. Papadopoulou, J. Batista, S. Hočevar, H. K. Matralis, *Catal. Today* **2002**, *75*, 157–167.
19. G. Sedmak, S. Hočevar, J. Levec, *J. Catal.* **2003**, *213*, 135–150.
20. D. H. Kim, J. E. Cha, *Catal. Lett.* **2003**, *86*, 107–112.
21. G. Sedmak, S. Hočevar, J. Levec, *J. Catal.* **2004**, *222*, 87–99.
22. G. Sedmak, S. Hočevar, J. Levec, *Topics in Catalysis* **2004**, *30–31*, 445–449.
23. Y. Liu, T. Hayakawa, K. Suzuki, S. Hamakawa, T. Tsunoda, T. Ishii, M. Kumagai, *Appl. Catal. A* **2002**, *223*, 137–145.
24. Y. Liu, T. Hayakawa, T. Tsunoda, K. Suzuki, S. Hamakawa, K. Murata, R. Shiozaki, T. Ishii, M. Kumagai, *Topics in Catalysis* **2003**, *22*, 205–213.
25. J. Papavasillou, G. Avgouropoulos, T. Ioannides, *Catal. Commun.* **2004**, *5*, 231–235.
26. Lj. Kundakovic, M. Flytzani-Stephanopoulos, *Appl. Catal. A* **1998**, *171*, 13–29.

27. P. Zimmer, A. Tschöpe, R. Birringer, *J. Catal.* **2002**, *205*, 339–345.
28. A. Tschöpe, J. Y. Ying, *Nanostruct. Mater.* **1994**, *4*, 617–623.
29. J. Y. Ying, A. Tschöpe, D. Levin, *Nanostruct. Mater.* **1995**, *6*, 237–246.
30. B. Skarman, T. Nakayama, D. Grandjean, R. E. Benfield, E. Olsson, K. Niihara, L. R. Wallenberg, *Chem. Mater.* **2002**, *14*, 3686–3699.
31. A. B. P. Lever, *Inorganic Electronic Spectroscopy*; Elsevier: Amsterdam, 1984.
32. C. Lamonier, A. Bennani, A. D´Huysser, A. Aboukaïs, G. Wrobel, *J. Chem. Soc., Faraday Trans.* **1996**, *92*, 131–136.
33. G. Wrobel, C. Lamonier, A. Bennani, A. D´Huysser, A. Aboukaïs, *J. Chem. Soc., Faraday Trans.* **1996**, *92*, 2001–2009.
34. J. L. G. Fierro, J. Soria, J. Sanz, J. M. Rojo, *J. Solid State Chem.* **1987**, *66*, 154–162.
35. A. Tschöpe, M. L. Trudeau, J. Y. Ying, *J. Phys. Chem. B* **1999**, *103*, 8858–8863.
36. G. Fierro, M. Lo Jacono, M. Inversi, P. Porta, R. Lavecchia, F. Cioci, *J. Catal.* **1994**, *148*, 709–721.
37. A. Aboukaïs, A. Bennani, C. F. Aissi, G. Wrobel, M. Guelton, *J. Chem. Soc., Faraday Trans.* **1992**, *88*, 1321–1325.
38. A. Pintar, J. Batista, S. Hočevár, *J. Coll. Interface Sci.*, in print.
39. H. C. Yao, Y. F. Yu Yao, *J. Catal.* **1984**, *86*, 254–265.
40. Powder Diffraction File; International Center for Diffraction Data, Newtown, 2000.
41. H. P. Klug, L. E. Alexander, *X-Ray Diffraction Procedures (For Polycrystalline and Amorphous Materials)*; Wiley & Sons: New York, 1954, p. 491 ff.

## Povzetek

Sintetizirali smo nanokristalinični  $(\text{CuO})_{0.15}(\text{CeO}_2)_{0.85}$  oksid po sol-gel metodi z uporabo vodikovega peroksida. Redoks lastnosti oksidnega vzorca smo preučevali s temperaturno programiranimi tehnikami redukcije (TPR), oksidacije (TPO) in desorpcije (TPD). Rezultati analiz so pokazali, da se pri redukciji CuO, ki je dispergirana na površini  $\text{CeO}_2$  nanokristalitov, zniža specifična površina  $(\text{CuO})_{0.15}(\text{CeO}_2)_{0.85}$  oksida, medtem ko celotna poraba vodika v zaporedno izvedenih TPR/TPO ciklih ostane konstantna. To pomeni, da se visoka stopnja disperzije CuO ohrani celo po aglomeraciji  $\text{CeO}_2$  nanokristalitov v gostejšo sekundarno strukturo. Med TPR procesom poteče popolna redukcija CuO v  $\text{Cu}^0$  in na površini delno reduciranega  $\text{CeO}_2$  se tvorijo skupki kovinskih delcev. V TPO stopnji naknadno poteče popolna reoksidacija  $\text{Cu}^0$  in ponovna disperzija nastalega CuO na površini  $\text{CeO}_2$  kristalitov.